Electronic Supplementary Material (ESI) for Energy & Environmental Science.
This journal is © The Royal Society of Chemistry 2017

Electronic Supplementary Material (ESI) for Energy & Environmental Science

Controlled Red Phosphorus@Ni-P Core@Shell Nanostructure as an Ultralong Cycle-Life and Superior High-Rate Anode for Sodium-Ion Batteries

Shuai Liu[a], Jinkui Feng*[a], Xiufang Bian*[a], Jie Liu[b], Hui Xu[a] and Yongling An[a]

[a] *Key Laboratory for Liquid-Solid Structural Evolution and Processing of Materials (Ministry of Education), School of Materials Science and Engineering, Shandong University, Jinan 250061, China*

[b] *Advanced Fibers &Modern Textile Cultivation Base of State Key Lab, Qingdao University, Qingdao 266071, China*

Experimental Section

1. Material synthesis

The RP powders (99.9 wt%, Aladdin Industrial Co., Ltd.) were sensitized in 10 g L^{-1} $SnCl_2$ (99 wt%, Aladdin Industrial Co., Ltd.) solution and subsequently activated in 0.5 g L^{-1} $PdCl_2$ (AR, Sinopharm Chemical Reagent Co. Ltd) solution before electroless deposition. The electroless

---

*Corresponding author.
E-mail address: jinkui@sdu.edu.cn (J. K. Feng); xfbian@sdu.edu.cn (X.F. Bian)

deposition of Ni-P alloys were performed in an acidic solution (pH=5.0), containing 25 g L^{-1} $NiSO_4 \cdot 6H_2O$ (99 wt%, Aladdin Industrial Co., Ltd.), 25 g L^{-1} $NaH_2PO_2 \cdot H_2O$ (99 wt%, Aladdin Industrial Co., Ltd.), 12 g L^{-1} CH_3COONa (99 wt%, Sinopharm Chemical Reagent Co. Ltd), and 28 mL L^{-1} lactic acid ($C_3H_6O_3$) (AR, Sinopharm Chemical Reagent Co. Ltd). Deposition took place in a thermostated vessel with a capacity of 500 cm^3 maintained at 80 °C for 30 min. After the electroless deposition, the dealloying of the RP@Ni-P was performed in a 5 wt% HCl aqueous solution with water bath at 60 °C for different time (from 1 to 20 h). The magnetic stirring (Model No. JJ-I) was at a rate of 600 r/min. Gas bubbles generated on the surface of the RP@Ni-P at the beginning of the dealloying reaction which finished when no bubbles emerged in the HCl solution. After dealloying, the precipitation was filtered with filter paper and rinsed with distilled water for several times, followed by drying for 24 h at 60 °C under vacuum. The as-prepared samples were kept in a vacuum chamber to avoid oxidation. The electroless deposition Ni on Cu current collector was directly performed in the electroless plating solution above at 80 °C for 30 min without the treatment with $SnCl_2$ and $PdCl_2$ solution. The mass loading of the Ni coating on Cu current collector is about 12.2 mg. The mass of the Cu current collector we used is 13.4 mg.

2. Sample Characterization

The microstructure of the prepared sample was characterized by scanning emission microscope (SEM, HITACHI SU-70), high resolution transmission electron microscope (HRTEM, JEOL JEM-2100). After the cycled electrodes at full charge state were taken out from the half-cell, the microstructure of the cycled electrodes was characterized by SEM. The structure and composition were characterized using X-ray diffraction (XRD, Rigaku Dmax-rc diffractometer), LabRAM HR800 spectrometer for Raman spectra, Tensor 27 for Fourier transform infrared spectroscopy (FT-IT, Bruker) and ESCALAB 250 for X-Ray Photoelectron Spectroscopy (XPS, ThermoFisher SCIENTIFIC). The actual content of Ni in the sample was determined by inductive coupled plasma atomic emission spectrometry (ICP-AES, Perkin Elmer 7300DV). The electronic conductivity was measured by four-point probe method (ET-9000, East Changing).

3. Electrochemical Measurements

The as-prepared active material was mixed with super P (purchased from lzy battery sales department in China) and a carboxymethyl cellulose (CMC) binder (70 : 15 : 15 in weight) in deionized water to form a homogenous slurry, which was painted on a copper foil (purchased from lzy battery sales department in China) and then dried at 80 °C under vacuum for 12 h to form the electrodes. The mass loading of active materials in RP, RP@Ni-P, 1h RP@Ni-P, 4h RP@Ni-P, 8h RP@Ni-P, 10h RP@Ni-P and 20h RP@Ni-P electrode are about 1.96 mg, 2.51 mg, 2.43 mg, 2.41 mg, 2.38 mg, 2.17 mg and 2.03 mg, respectively. Na sheet (home-made) was used as the counter electrode, and Celgard 2400 was used as the separator. The electrolyte was a mixture of 1 M $NaClO_4$ in propylene carbonate with 5% fluoroethylene carbonate (FEC) additive. All the cells (CR2016 coin-type) (purchased from lzy battery sales department in China) were assembled in a glove box with water/oxygen content lower than 1 ppm and tested at room temperature. Cyclic voltammetric measurements were carried out with the coin cells at a scan rate of 0.1 mV s^{-1} between 0.05 and 2.5 V (vs. Na^+/Na) using a CHI 660E electrochemical workstation (Shanghai, China). Galvanostatic discharge/charge cycles were performed between 0.05 and 2.0 V (vs. Na^+/Na) on a Neware-CT-3008 test system (Shenzhen, China). Electrochemical impedance spectroscopy (EIS) was also performed on a CHI 660E electrochemical workstation with a frequency of 100 kHz to 0.01 Hz. For the Na ion full cell, homemade $Na_3V_2(PO_4)_3/C$,[1] acetylene black, and poly (vinylidene fluoride) (PVDF) in a weight ratio of 75:15:10 were used to fabricate the cathode using Al foil as the current collector. For the full cells, the excess capacity of cathode was controlled at ~10% while the anode was limited.[2]

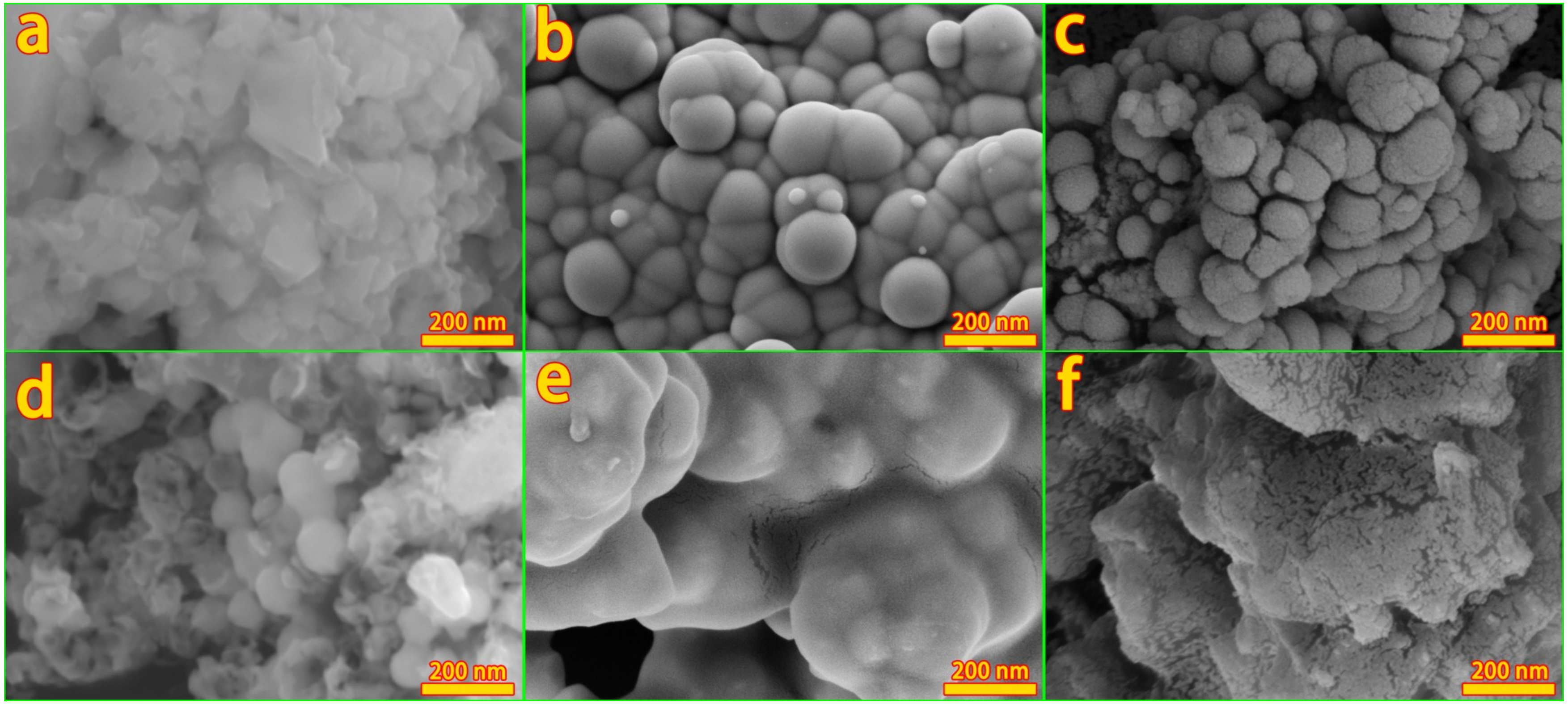

Fig. S1 SEM images of RP nanoparticles (a) and RP@Ni-P core@shell nanostructure (electroless deposition Ni on RP) (b). (c)-(f) SEM images of RP@Ni-P immersed in the HCl solution for 1 h (c), 4 h (d), 8 h (e) and 10 h (f), respectively.

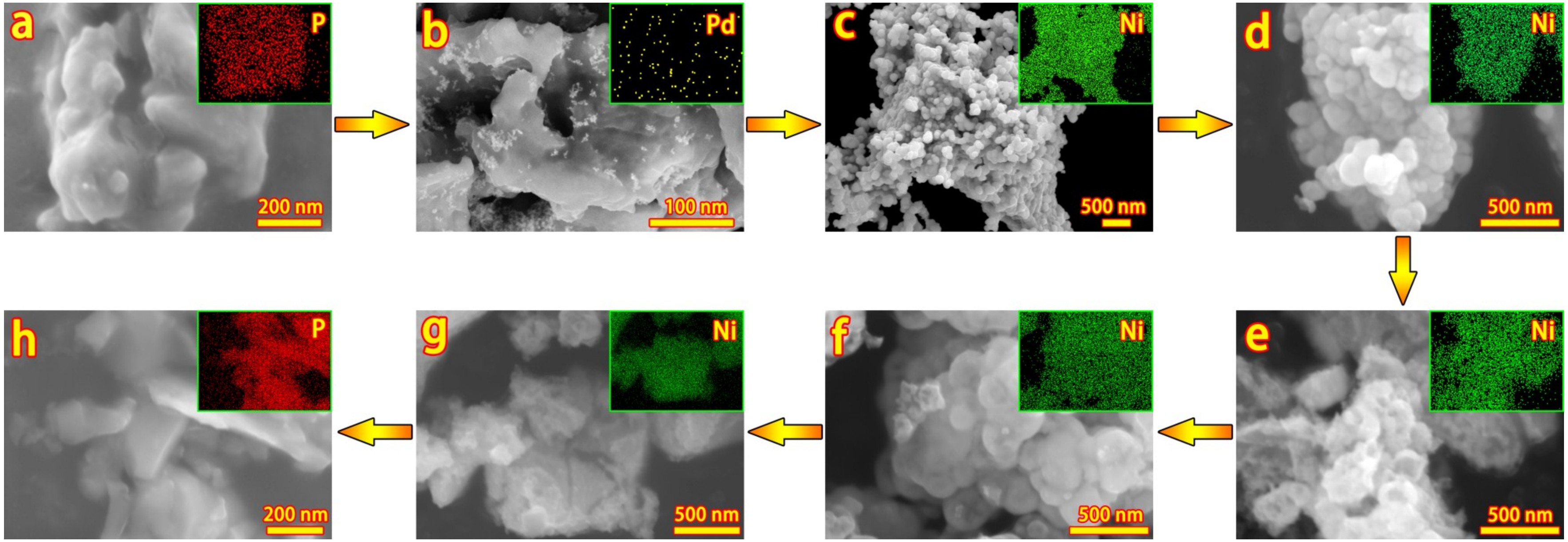

Fig. S2 (a) SEM image of RP with EDX mapping of elemental P in the inset. (b) SEM image of RP coated with few Pd catalyst with EDX mapping of elemental Pd in the inset. (c) SEM image of RP@Ni-P before dealloying with EDX mapping of elemental Ni in the inset. (d-g) SEM images of RP@Ni-P (RP@Ni-P immersed in the HCl solution for 1 h (d), 4 h (e), 8 h (f) and 10 h (g), respectively) with EDX mapping of elemental Ni in the insets. (h) SEM image of RP@Ni-P immersed in the HCl solution for 20 h with EDX mapping of elemental P in the inset.

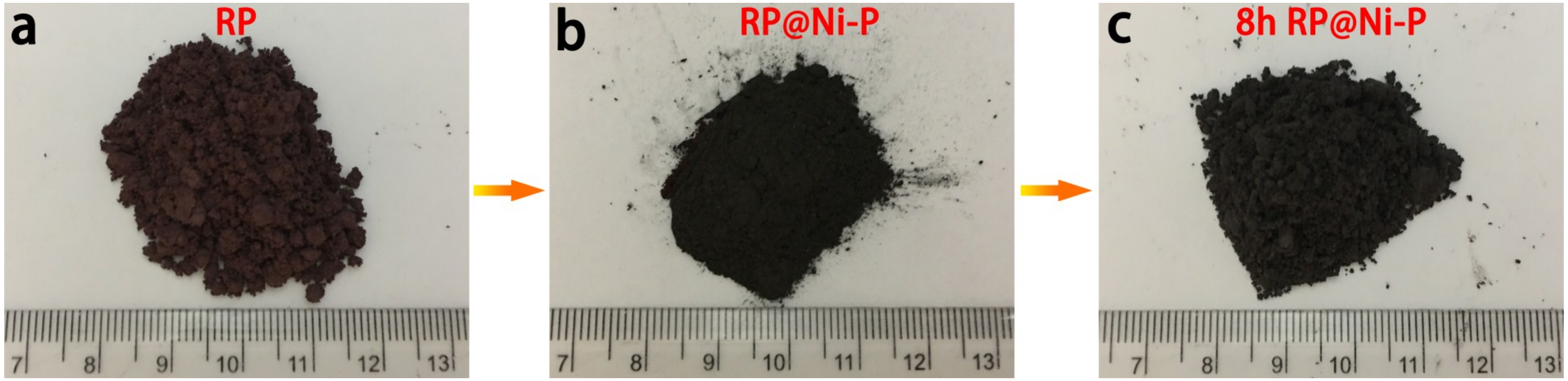

Fig. S3 Photograph evolution of RP powder (a), RP@Ni-P powder (b) and 8h RP@Ni-P powder (RP@Ni-P immersed in the HCl solution for 8 h) (c).

As shown in Fig. S3, the RP powder (a) is dark red before electroless deposition Ni on it. The RP@Ni-P powder (b) is black because of the Ni-P shell on RP nanoparticles. After immersing RP@Ni-P powder in the HCl solution for 8 h (8h RP@Ni-P) (c), the colour of the powder is still black due to the thin Ni-P shell on the RP surface.

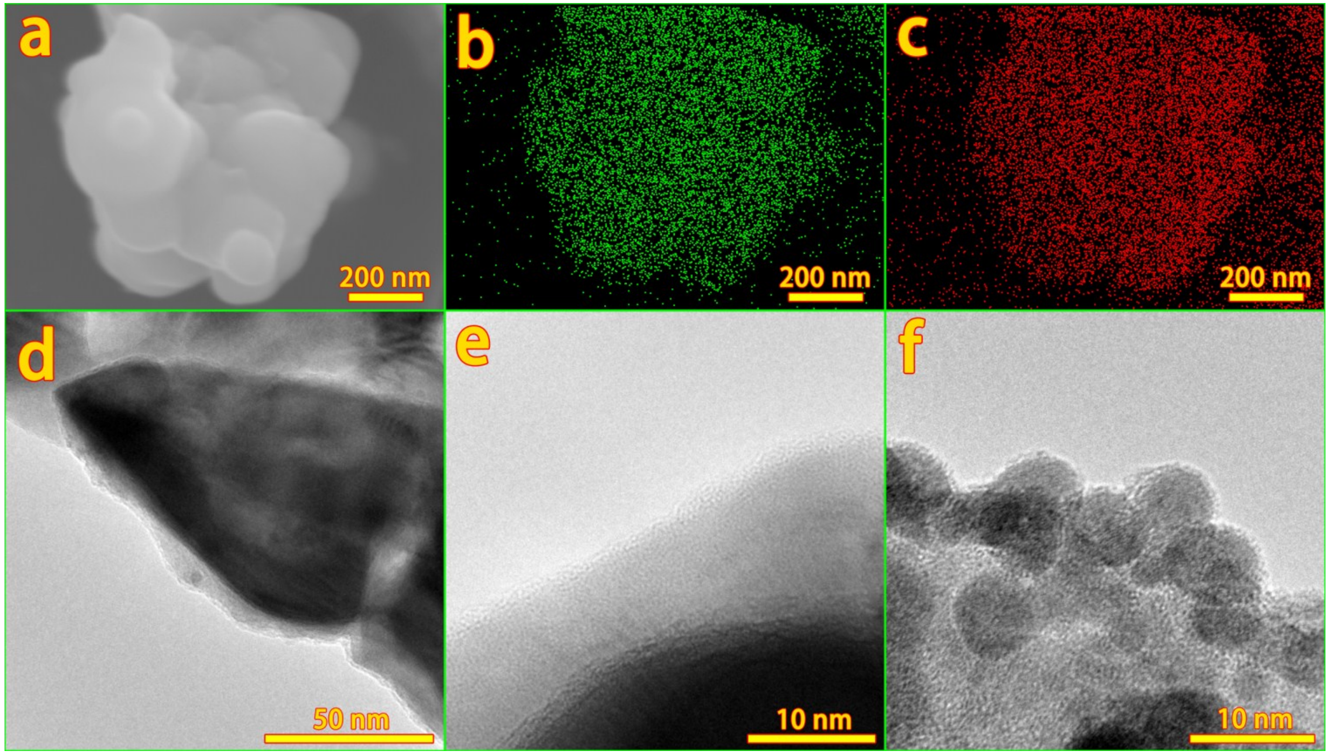

Fig. S4 (a) SEM image and corresponding (b) Ni and (c) P EDX element mapping of 8h RP@Ni-P. (d) and (e) High resolution TEM (HRTEM) images of 8h RP@Ni-P. (f) HRTEM image of 10h RP@Ni-P.

As indicated in SEM image (Fig. S4a), corresponding Ni (b) and P (c) EDX element mapping and HRTEM images of 8h RP@Ni-P, the RP cores are coated by continuous and uniformly Ni-P shell, which can not only inhibit the large volume expansion of RP efficiently, but also facilitate transmission of Na ions and electrons during sodiation-desodiation process. As shown in the high-resolution TEM (HRTEM) images of 10h RP@Ni-P (Fig. S4f), after immersion in the HCl solution for 10 h, the in-situ generated Ni_2P crystalline grains with a thin amorphous outer shell (thickness ~2 nm) are embed on the amorphous RP substrate while most of the RP substrate exposes due to the thin defective Ni-P shell etched by the HCl solution.

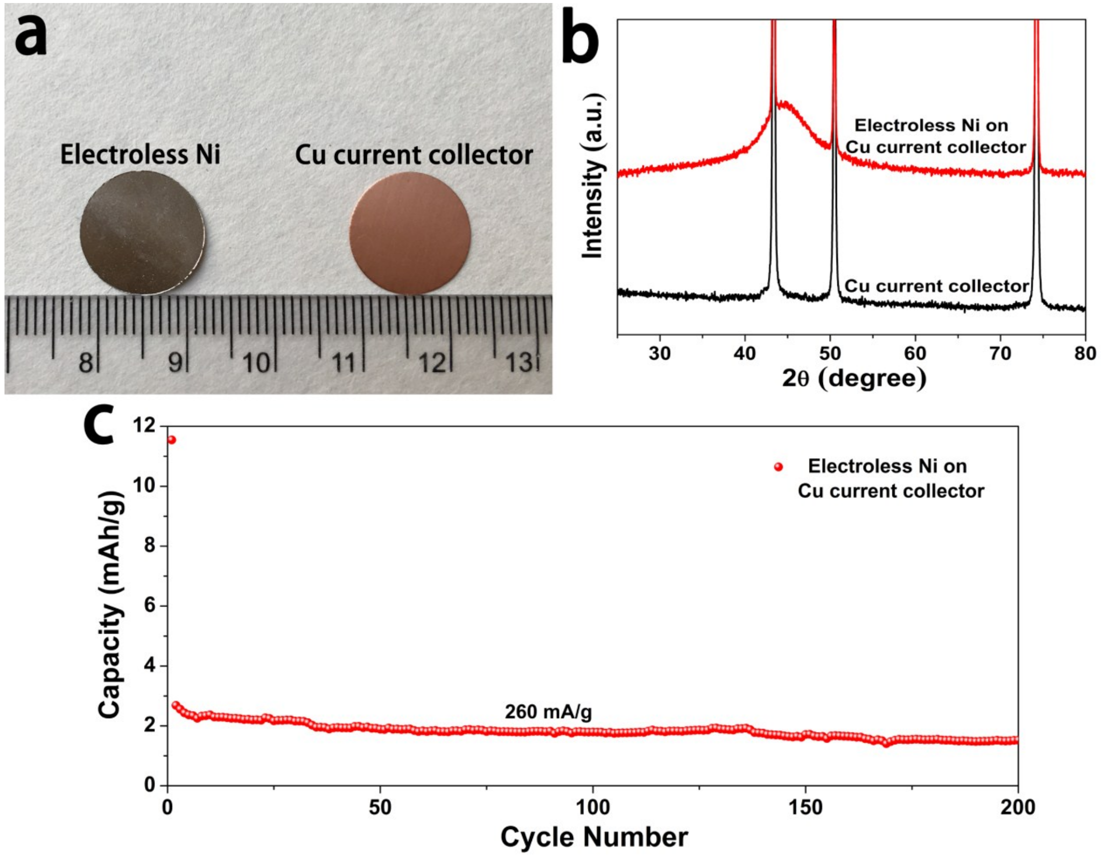

Fig. S5 (a) Photograph of Cu current collector (right) and electroless deposition Ni on Cu current collector (left). (b) XRD patterns of Cu current collector and electroless deposition Ni on Cu current collector. (c) Cycling performance of the electroless deposition Ni (on Cu current collector) electrodes at a current density of 260 mA/g.

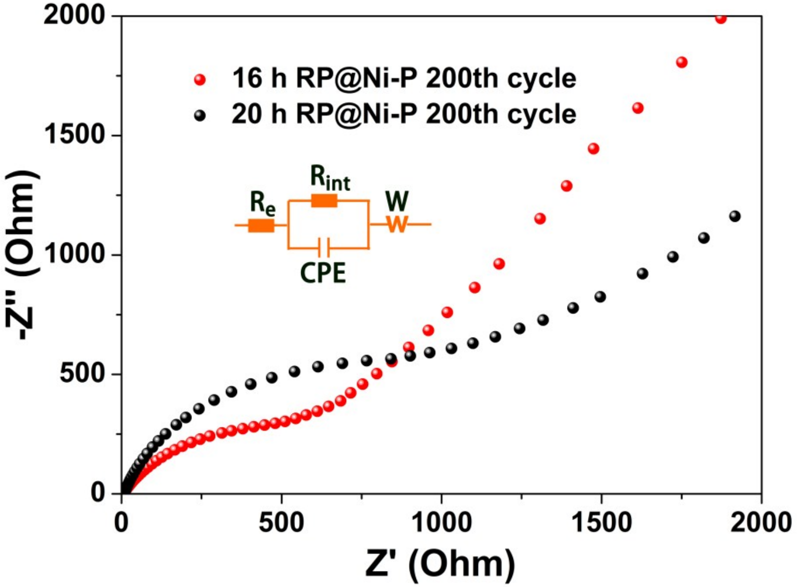

Fig. S6 Nyquist plots of the 16h RP@Ni-P electrodes and 20h RP@Ni-P electrodes after 200 cycles at full charge state (galvanostatic discharge/charge at a current density of 260 mA/$g_{composite}$ between voltage of 0.05 and 2.0 V).

The Nyquist plots of electrodes in Fig. S5 consist of a single depressed semicircle in the high-medium frequency region and an inclined line at the low frequency. According to our previously study and literature, the semicircle in EIS spectra relates to the composited impedance of Na-ion transport through surface film and charge transfer at the electrode/electrolyte interface.[3-12] The value of R_e (17.8 Ω) and R_{int} (583.2 Ω) of 16 h RP@Ni-P with little Ni_2P on the surface is smaller than that of 20h RP@Ni-P (R_e=23.2 Ω, R_{int}=1282.7 Ω) without Ni_2P after 200 cycles, as shown in Table S1.

Table S1 Kinetic parameters of RP, RP@Ni-P, 8h RP@Ni-P, 10h RP@Ni-P, 16h RP@Ni-P and 20h RP@Ni-P electrodes.

Sample	R_e (Ω)	R_{int} (Ω)
RP	29.7	1521.6
RP@Ni-P	15.1	517.4
8h RP@Ni-P	8.8	310.9
10h RP@Ni-P	9.1	371.3
16h RP@Ni-P	17.8	583.2
20h RP@Ni-P	23.2	1282.7

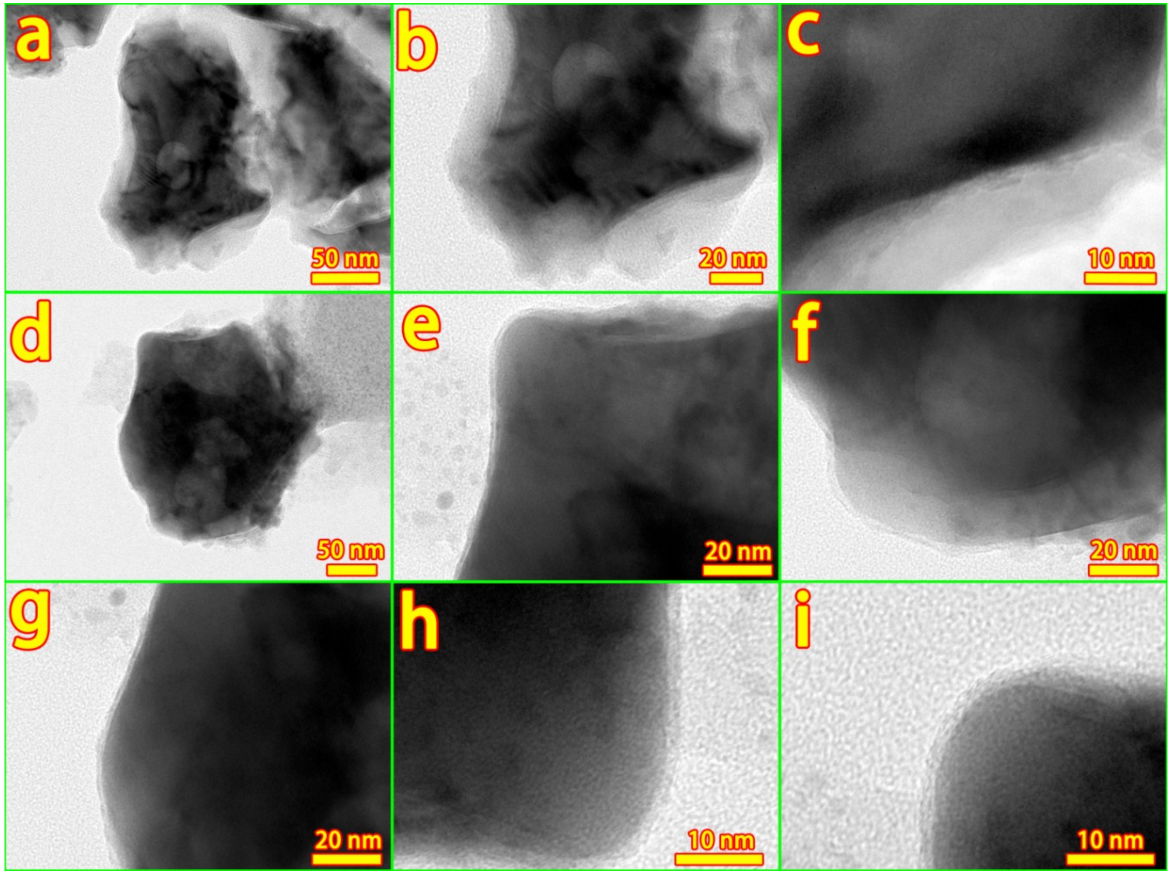

Fig. S7 (a), (b) and (c) HRTEM images of the 8h RP@Ni-P electrodes after first discharge and charge process. (d) TEM image and (e-i) HRTEM images of the 8h RP@Ni-P electrodes after 2000 cycles at full charge state at a current density of 5 A/$g_{composite}$ between 0.05 and 2.0 V.

The core@shell structure of 8h RP@Ni-P before (Fig. 3b-e and Fig. S4d-e) and after first cycle (Fig. S7a-c) is almost unchanged. The uncracked 8h RP@Ni-P core@shell nanostructure could maintain after long term charge-discharge process (2000 cycles) because of the Ni-P outside shell which enables intimate electrical contact of RP and current collector, and tolerance for successive volume change of RP upon cycling. The shell thickness of 8h RP@Ni-P after 2000 cycles become thinner than that of 8h RP@Ni-P after first cycle, which may be caused by long term sodiation-desodiation process and chemical reaction with electrolyte.

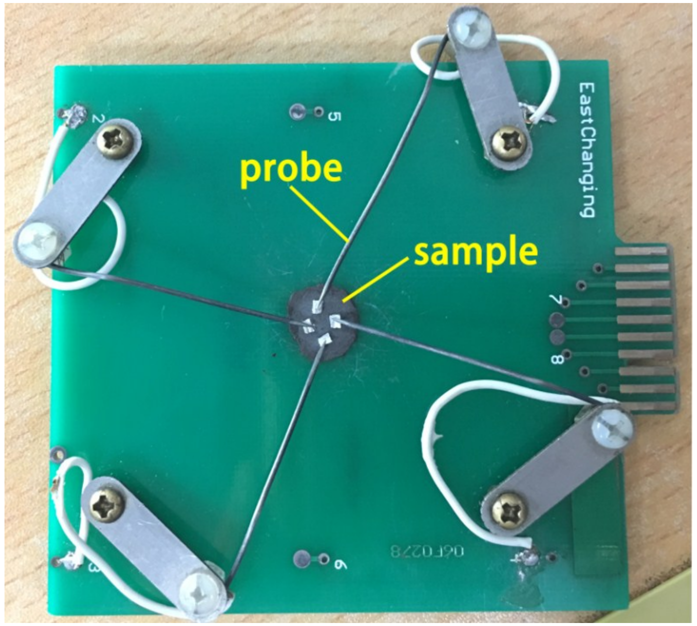

Fig. S8 Electronic conductivity of Pd coated RP, RP@Ni-P, 8h RP@Ni-P and 10h RP@Ni-P is measured with four-point probe method.

As we know, low electronic conductivity (~10^{-14} S/cm) is a big issue for RP anode. The electronic conductivity of the Pd coated RP is 3.55×10^{-2} S/cm, much higher than that of RP, which will facilitate the improvement of sodium storage performance. Ni-P coating on P particles will further facilitate the improvement of the electrical conductivity greatly. Generally, more thick Ni-P coating layer, higher the electrical conductivity. As a result, the sequence of electronic conductivity is RP@Ni-P (1.78 S/cm) > 8h RP@Ni-P (1.23 S/cm) > 10h RP@Ni-P (0.56 S/cm).

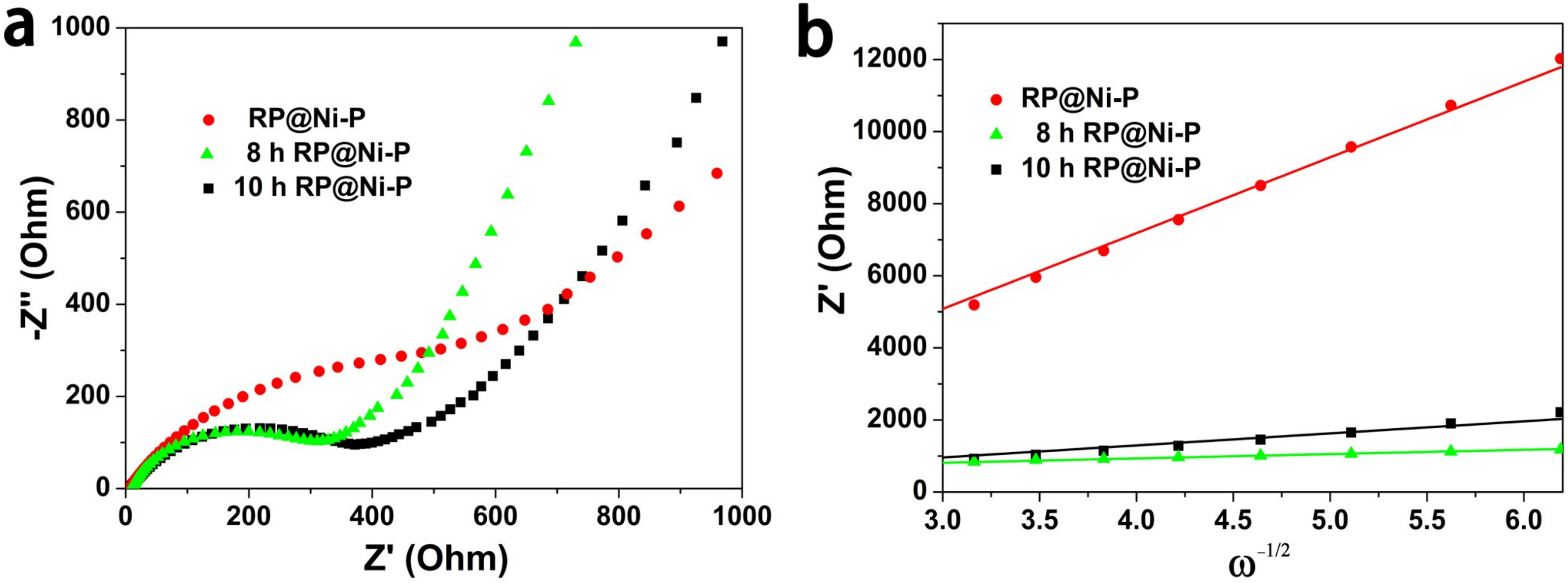

Fig.S9 (a) Nyquist plots of RP@Ni-P, 8 h RP@Ni-P and 10 h RP@Ni-P. (b) Fitting of the coefficient of Warburg impedance (σ_w) from the linear fitting line of Z' versus $\omega^{-1/2}$.

As shown in Fig. S9a, the curves in the frequency region show Warburg impedance with distinctly different slopes, indicating the electrodes possess different solid-state ion diffusion behaviors. Fig. S9b shows the fitting results of the coefficient of Warburg impedance (σ_w), in which there is an obvious lower Z' versus $\omega^{-1/2}$ slope of 8 h RP@Ni-P than that of RP@Ni-P. With aforementioned concerns, the Na^+ diffusion characteristics were calculated by Equation (1)[13, 14]:

$$D = \frac{R^2T^2}{2A^2n^4F^4C^2\sigma_w^2} \quad (1)$$

Where R is the gas constant, T is the absolute temperature, A is the surface area of the electrode, n is the number of electrons involved in the intercalation process, F is the Faraday constant, and C is the molar concentration of Na^+ in the sample. As a result, 8h RP@Ni-P possesses a higher Na^+ diffusion coefficient of 8.22×10^{-14} cm^2/s than 10h RP@Ni-P (1.04×10^{-14} cm^2/s) , which is two orders of magnitude higher than that of RP@Ni-P (2.68×10^{-16} cm^2/s).

Table S2 Comparison of Electronic conductivity and Na^+ Diffusion coefficient of RP@Ni-P with different Ni content.

Sample	**Ni content** (wt%)	**Electronic conductivity** (S/cm)	**Na^+ Diffusion coefficient** (cm^2/s)
RP@Ni-P	15.29	1.78	2.68×10^{-16}
8 h RP@Ni-P	6.17	1.23	8.22×10^{-14}
10 h RP@Ni-P	3.36	0.56	1.04×10^{-14}

There should be a balance between the electronic conductivity and ion conductivity for the RP@Ni-P with different shell thickness. The sequence of electronic conductivity is RP@Ni-P (1.78 S/cm) > 8h RP@Ni-P (1.23 S/cm) > 10h RP@Ni-P (0.56 S/cm). However, 8h RP@Ni-P possesses a Na^+ diffusion coefficient of 8.22×10^{-14} cm^2/s, which is two orders of magnitude higher than that of RP@Ni-P (2.68×10^{-16} cm^2/s). It further confirms the superior cycling performance of 8h RP@Ni-P electrodes.

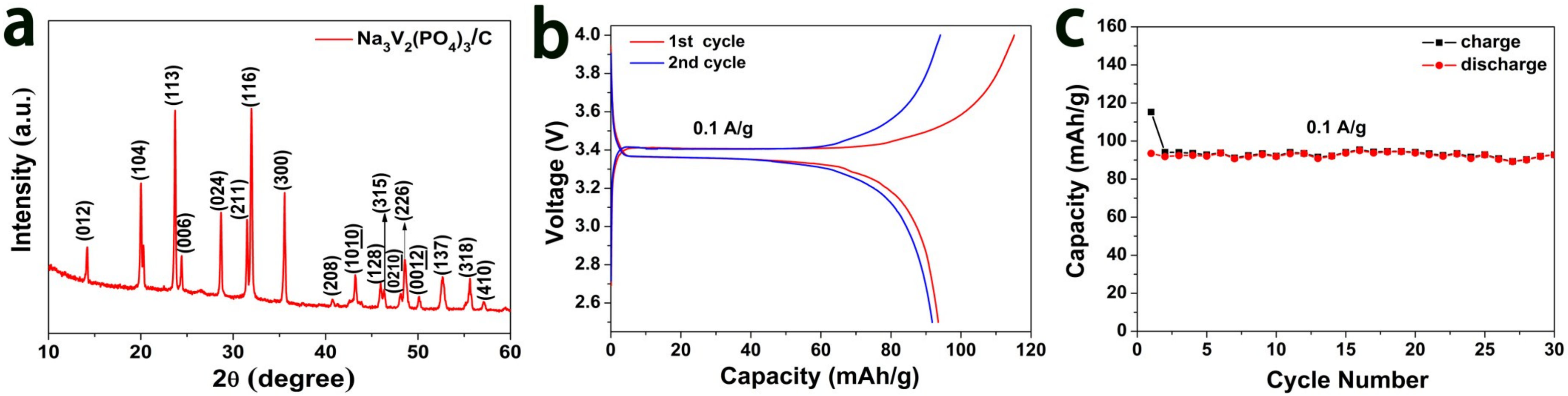

Fig. S10 (a) XRD pattern of the home-made $Na_3V_2(PO_4)_3$/C. (b) Charge-discharge curves and (c) cycling performance of $Na_3V_2(PO_4)_3$/C at a current density of 0.1 A/g within 2.5-4.0 V.

Here, $Na_3V_2(PO_4)_3$/C (Fig. S10a) is home-made by sol-gel procedure.[1] As shown in Fig. S10b-c, the $Na_3V_2(PO_4)_3$/C could stabilize at a specific capacity of ~90 mAh/g at 0.1 A/g.

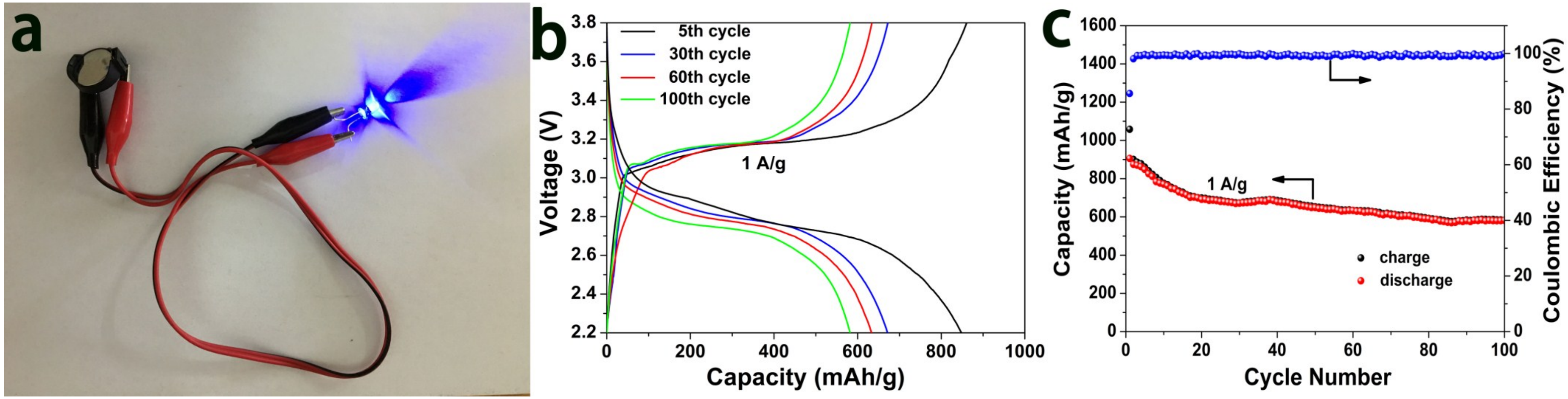

Fig. S11 (a) Digital image of the light-emitting diode (LED) lit by 8h RP@Ni-P // $Na_3V_2(PO_4)_3$/C full cell. (b) Discharge/charge curves and (c) cycling performance at 1 A/g within 2.2-3.8 V of this full battery, where only the mass of anode, 8h RP@Ni-P, is taken into account to calculate current density and gravimetric capacity.

Fig. S11 presents the cycling performance of the full cell within 2.2-3.8 V at a current density of 1 A/g_{anode}. As shown in Fig. S11b, the voltage profiles of both sodiation and desodiation processes are perfectly reproducible from 5 to 100 cycles, indicating the excellent electrochemical reversibility of the cell during cycling. Fig. S11c presents that the cell still preserves a discharge capacity of 581.8 mAh/g_{anode} and a high coulombic efficiency after 100 cycles. The capacity loss in the first several cycles can be ascribed to the SEI film formation and partly irreversible utilization of Na^+ by $Na_3V_2(PO_4)_3$/C cathode.[2, 15] The output voltage of the full cell is about 2.8 V. Compared to the previous reports about Na-ion full batteries ($Na_3V_2(PO_4)_3$/C // Sb@Ti-O-P, 2.72 V and 392 mAh/g_{anode} after 150 cycles;[2] $Na_3V_2(PO_4)_3$ // MoO_3, 1.4 V and 164 mAh/g_{anode} after 14 cycles;[16] $Na_3V_2(PO_4)_3$ // $FeSe_2$, 1.7 V and 298 mAh/g_{anode} after 150 cycles at 1 A g^{-1};[17] and $Na_{0.8}Ni_{0.4}Ti_{0.6}O_2$ // $Na_{0.8}Ni_{0.4}Ti_{0.6}O_2$, 2.8 V and 85 mAh/$g_{anode}$ after 150 cycles at 100 mA/g_{anode}[18]), the output voltage and cycling capacity have been improved by a lot by RP@Ni-P // $Na_3V_2(PO_4)_3$/C, indicating the promising potential for it to be used in sodium ion batteries.

Notes and references

1. M. J. Aragón, J. Gutiérrez, R. Klee, P. Lavela, R. Alcántara and J. L. Tirado, *J Electroanal Chem*, 2017, **784**, 47-54.
2. N. Wang, Z. Bai, Y. Qian and J. Yang, *Acs Appl Mater Interfaces*, 2017, **9**, 447-454.
3. S. Liu, J. Feng, X. Bian, J. Liu and H. Xu, *Energy & Environmental Science*, 2016, **9**, 1229-1236.
4. S. Liu, J. Feng, X. Bian, Y. Qian, J. Liu and H. Xu, *Nano Energy*, 2015, **13**, 651-657.
5. Y. Zhu, Y. Wen, X. Fan, T. Gao, F. Han, C. Luo, S.-C. Liou and C. Wang, *ACS Nano*, 2015, **9**, 3254-3264.
6. J. Song, Z. Yu, M. L. Gordin, X. Li, H. Peng and D. Wang, *ACS Nano*, 2015, **9**, 11933-11941.
7. S. Liu, J. Feng, X. Bian, J. Liu and H. Xu, *Journal of Materials Chemistry A*, 2016, **4**, 10098-10104.
8. J. Sun, G. Y. Zheng, H. W. Lee, N. Liu, H. T. Wang, H. B. Yao, W. S. Yang and Y. Cui, *Nano Lett*, 2014, **14**, 4573-4580.
9. U. Kasavajjula, C. Wang and A. J. Appleby, *J Power Sources*, 2007, **163**, 1003-1039.
10. Y. Sharma, N. Sharma, G. V. Subba Rao and B. V. R. Chowdari, *Chem Mater*, 2008, **20**, 6829-6839.
11. S. Liu, J. Feng, X. Bian, J. Liu and H. Xu, *RSC Advances*, 2015, **5**, 60870-60875.

12. J. Song, Z. Yu, M. L. Gordin, S. Hu, R. Yi, D. Tang, T. Walter, M. Regula, D. Choi, X. Li, A. Manivannan and D. Wang, *Nano Lett*, 2014, **14**, 6329-6335.
13. Y. Tang, Y. Zhang, X. Rui, D. Qi, Y. Luo, W. R. Leow, S. Chen, J. Guo, J. Wei, W. Li, J. Deng, Y. Lai, B. Ma and X. Chen, *Adv Mater*, 2016, **28**, 1567-1576.
14. H. He, G. Jin, H. Wang, X. Huang, Z. Chen, D. Sun and Y. Tang, *Journal Of Materials Chemistry A*, 2014, **2**, 3563-3570.
15. N. Wang, Z. Bai, Y. Qian and J. Yang, *Adv Mater*, 2016, **28**, 4126-4133.
16. S. Hariharan, K. Saravanan and P. Balaya, *Electrochem Commun*, 2013, **31**, 5-9.
17. K. Zhang, Z. Hu, X. Liu, Z. Tao and J. Chen, *Adv Mater*, 2015, **27**, 3305-3309.
18. S. Guo, H. Yu, P. Liu, Y. Ren, T. Zhang, M. Chen, M. Ishida and H. Zhou, *Energy & Environmental Science*, 2015, **8**, 1237-1244.